ULF Wave Generation Through Particle Precipitation Induced by VLF Transmitters

T. F. BELL

Radioscience Laboratory, Stanford University, Stanford, California 94305

Recent experiments have shown that significant fluxes (10^{-1} erg/cm^2 s) of energetic electrons can be precipitated into the ionosphere at times when VLF emissions are triggered in the magnetosphere by whistlers. If similar fluxes can be produced during the artificial triggering of VLF emissions by ground- or satellite-based VLF transmitters, then a powerful tool would be available for studying the dynamics of the lower ionosphere. In the present paper we explore the feasibility of a technique to stimulate ULF waves in the ionosphere using the tool of controlled particle precipitation. Periodic (period of $>\frac{1}{2}$ s) transmissions from a VLF ground-based transmitter are used to trigger VLF emissions and precipitate energetic electrons. The periodic precipitated flux modifies the conductivity of the *D* and *E* regions, inducing periodic changes in current flow which in turn result in the generation of Pc 1 ULF waves. Calculations indicate that ULF wave amplitudes of 1 γ may be produced in this process. Furthermore, steady state magnetic field perturbations may reach 100 γ at ground level. Since both these amplitudes would be readily measurable with present techniques, the results lend plausibility to the idea of attempting to produce detectable ULF waves by using ground- or satellite-based VLF transmitters.

INTRODUCTION

At the present time a high-power (100 kW) variable frequency (1–20 kHz) VLF transmitter is in operation at Siple Station in the Antarctic. The main purpose of this transmitter is to perform controlled wave-particle interaction experiments in the magnetosphere [*Helliwell and Katsufrakis*, 1974] with the aim of determining the underlying physical processes which dictate the characteristics of energetic particles and waves in the magnetosphere. With understanding comes the possibility of control of these particles and the ability to (1) tap the energy of energetic particles to provide amplification of signals for the benefit of VLF communication and navigation systems, (2) increase or diminish the average energy of trapped energetic particles in the magnetosphere, (3) precipitate energetic particles out of the magnetosphere, and (4) study the physics of the aurora and the lower ionosphere by using controlled particle precipitation as a tool.

While some of these goals may prove difficult to accomplish, others are presently within reach. For instance, the amplification of VLF signals by energetic particles has been well documented and is presently under study, the Siple facility being used [*Stiles and Helliwell*, 1975]. Another goal apparently within reach is the controlled precipitation of energetic particles from the magnetosphere. The rationale for this belief is provided by recent experimental evidence which indicates that significant and readily detectable fluxes of energetic particles can be precipitated out of the magnetosphere by discrete VLF signals such as whistlers and VLF emissions [*Rosenberg et al.*, 1971; *Helliwell et al.*, 1973].

In these interactions the discrete signals appear to trigger a powerful natural instability in the energetic particle population, and the energy content of the precipitating particles is many orders of magnitude greater than the energy content of the triggering signal.

With the tremendous leverage available in an interaction of this kind, significant particle precipitation effects may be induced even by triggering signals of relatively low amplitude compared to typical whistlers and emissions. In particular, it may be possible to trigger these precipitation events by using a VLF transmitter such as that available at Siple Station. If this can be done, then a powerful tool would be available for the study of the physics of the lower ionosphere as well as the physics of the aurora and airglow.

An additional possible use of controlled particle precipitation lies in the artificial generation of ULF waves in the lower ionosphere, in particular, the type of ULF wave known as geomagnetic micropulsations. In general, micropulsations consist of short-period (0.1 s to 10 min) fluctuations of the earth's magnetic field. The origins of micropulsations are not clear, but they have important diagnostic applications to the structure of the magnetosphere.

Many previous proposals to generate micropulsations artificially have suffered from the fact that the size of effective radiating structures is so large (~100 km in scale) that construction of these structures is a major undertaking [*Fraser-Smith et al.*, 1972; *C. Greifinger*, 1972; *Fraser-Smith and Bubenik*, 1974; *Greifinger and Greifinger*, 1974]. It is the purpose of this paper to suggest a method whereby this handicap can be overcome and whereby the tool of controlled particle precipitation can be used to create large-scale ULF radiating structures in the lower ionosphere. The idea behind this method is that controlled particle precipitation can be used to vary the current flow periodically in the *E* and *D* regions of the ionosphere. This varying current then produces ULF radiation in the micropulsation frequency range. As one of the referees has pointed out, an analogous (but naturally occurring) mechanism has been proposed by *Campbell* [1967] to explain aurorally associated irregular pulsations of the natural electromagnetic field. If Campbell's theory is correct, the feasibility of our own plan would become more certain.

MODEL

The model of micropulsation generation which we wish to suggest is represented schematically in Figures 1–3. As is shown in Figure 1, a fixed frequency pulse of approximately $\frac{1}{2}$-s duration is injected through the ionosphere and into the magnetosphere from a high-power (100 kW) VLF transmitter located at mid-latitude (50°–60° invariant). This pulse follows the earth's magnetic field lines and subsequently arrives near the earth's magnetic equatorial plane and begins to interact strongly with energetic electrons through gyroresonance. In

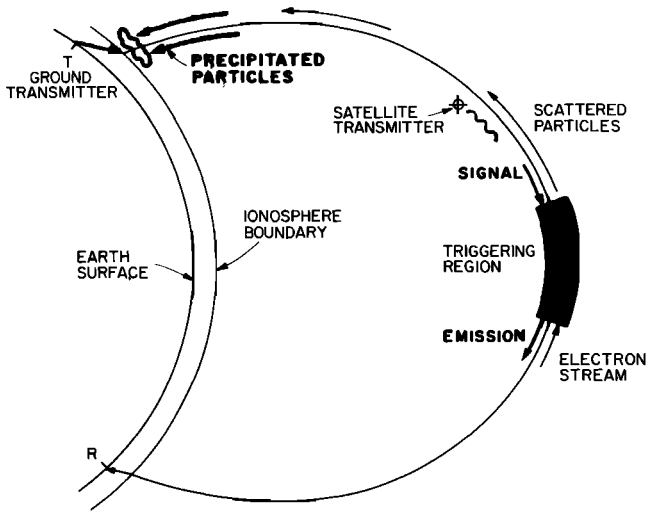

Fig. 1. Schematic representation of VLF wave injection experiment to produce particle precipitation. A pulse from a VLF ground transmitter (or satellite transmitter) is injected into the magnetosphere and follows the earth's static magnetic field lines to a region near the magnetic equatorial plane, where it begins to interact strongly with energetic electrons through gyroresonance. In the gyroresonance interaction, VLF emissions are produced, and numerous energetic electrons are scattered into the loss cone, proceed down the magnetic field lines, and precipitate into the ionosphere, where they create large-scale enhancements of ionization.

the gyroresonance interaction the injected wave amplitude may grow as much as 30 dB [*Stiles and Helliwell*, 1975], VLF emissions may be produced, and significant numbers of resonant energetic electrons are pushed into the loss cone. The loss cone electrons then proceed down the field lines and precipitate into the lower ionosphere, where they produce numerous secondary electrons and create an impulsive enhancement of ionization throughout the volume of the precipitation region, as is indicated schematically in Figure 2. In the volume of enhanced ionization the ionospheric conductivity (being proportional to the ionization density) is also enhanced, and the existence of an ambient electric field $\mathbf{E}_0$ being assumed, this initially produces an enhancement of the ionospheric currents flowing in the perturbed volume.

At the boundaries of the perturbed region, continuity of current requires that a polarization charge be built up. This charge gives rise to an electric field $\mathbf{E}_p$ which cancels a portion of $\mathbf{E}_0$ and also begins to drive currents both perpendicular and parallel to the earth's magnetic field lines $\mathbf{B}_0$. Because of the much higher conductivity along $\mathbf{B}_0$ the bulk of the current flows along $\mathbf{B}_0$. Thus the net effect of the increase in the conductivity in the precipitation region is to drive a current enhancement $\Delta\mathbf{I}$ through the perturbed region and along $\mathbf{B}_0$ toward the conjugate ionosphere. Field-aligned currents of this type that originate from conductivity variations have been called 'secondary Birkeland' currents [*Boström*, 1974]. The situation depicted in Figure 2 is the simple one in which both the electric field and the conductivity are constant throughout the perturbed volume. In this case, $\mathbf{E}_t = \mathbf{E}_0 - \mathbf{E}_p$ and $\Delta I = I_F = |\mathbf{I}_t - \mathbf{I}_0|$. The more general case, where $\mathbf{E}_t$ varies with altitude, is treated in Appendix A.

In the perturbed region the current enhancement produces an electromagnetic pulse whose spectrum contains a wide range of frequencies, most of which may lie outside the micropulsation range. However, if the VLF transmitter is programed to transmit a continuous train of pulses with a pulse repetition frequency in the micropulsation range, a large frac-

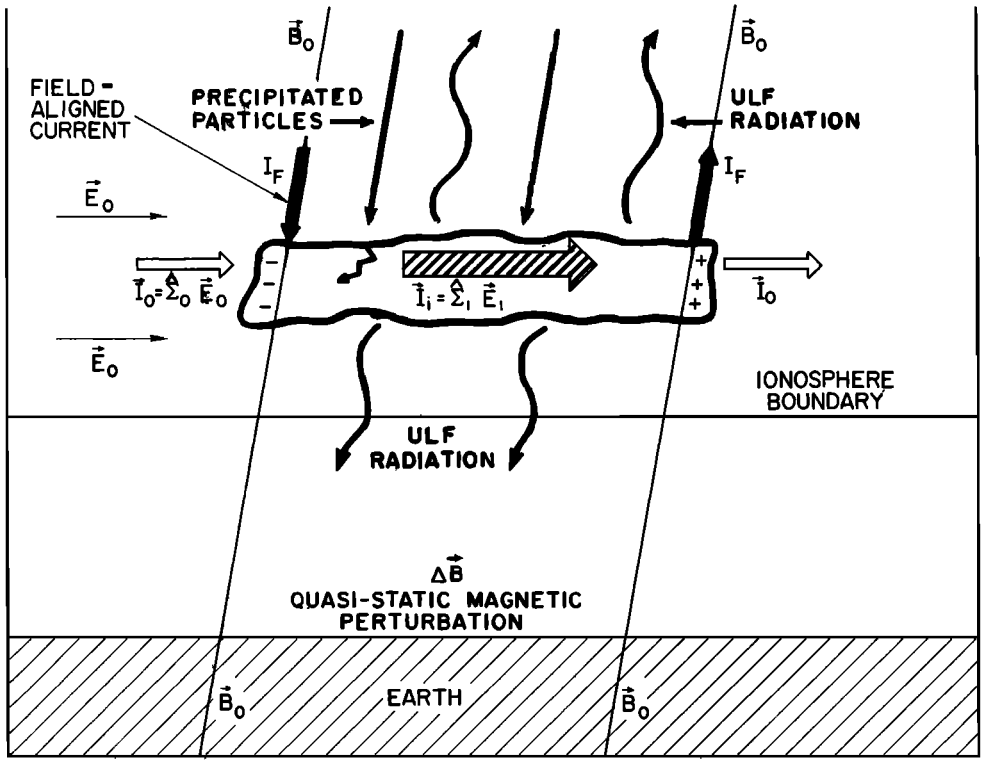

Fig. 2. Schematic two-dimensional representation of enhanced current flow in region of enhanced ionization produced by particle precipitation. The electric field inside the perturbation $\mathbf{E}_t$ is the sum of the ambient field $\mathbf{E}_0$ plus the polarization field $\mathbf{E}_p$. Periodic variation of the precipitated flux with approximately a 1-s period causes a periodic variation of current inside the perturbed region, leading to the radiation of ULF waves. Continuity of current is provided by a field-aligned current component I_F.

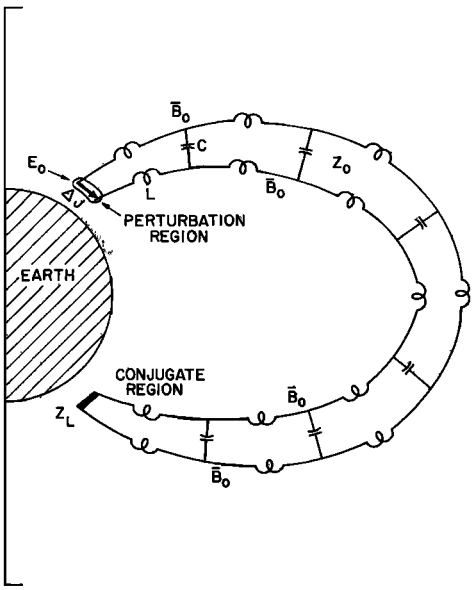

Fig. 3. Two-dimensional schematic representation of ULF wave transmission line linking the perturbed and conjugate ionospheres.

tion of the coherent radiation from the variable ionospheric current in the precipitation region will be within the micropulsation range.

In our model the current flow along $\mathbf{B}_0$ is described by using a transmission line analogy: the field lines threading the boundaries of the perturbed region and carrying the field-aligned currents are the guiding surfaces of the transmission line; the termination of the line is the resistive impedance of the conjugate ionosphere; and the source of the transmission line waves is the current ΔJ injected into the line in the perturbation region. A two-dimensional schematic representation of the proposed transmission line is shown in Figure 3 and discussed in Appendix A.

The current ΔJ which results from each burst of precipitated particles is directly proportional to $|\mathbf{E}_t|$ in the perturbed region. Initially, $\mathbf{E}_t$ is just the ambient field, but as the precipitation continues, the polarization charge ρ_p on the boundaries of the perturbed region may build up to such an extent that $|\mathbf{E}_t| \ll |\mathbf{E}_0|$. In this case, ΔJ will be minimized.

Because of the high value of the conductivity parallel to $\mathbf{B}_0$, $\rho_p > 0$ only if the current flow along $\mathbf{B}_0$ is limited. Consequently, if the ionosphere acts as a constant voltage source across the perturbed region, then $\rho_p \simeq 0$, $\mathbf{E}_t$ will remain approximately equal to $\mathbf{E}_0$, and ΔJ will be maximized. On the other hand, if the ionosphere acts as a constant current source across the perturbed region, the polarization charge can build up, and both $\mathbf{E}_t$ and ΔJ may be reduced. In our model we take the more conservative approach and assume that the ionosphere acts as a constant current source. With this assumption the value of $\mathbf{E}_t$ and ΔJ in the 'steady state' will depend upon the magnitude of the current that can be drawn from the conjugate ionosphere.

Particle Precipitation

The feasibility of our ULF wave generation plan depends upon the amount of particle precipitation that can be produced by a ground-based VLF transmitter. Unfortunately, to date, this quantity is unknown. However, we can make a rough estimate of this parameter using results of a recent experiment [*Rosenberg et al.*, 1971; *Foster*, 1973] in which Bremsstrahlung X ray fluxes were measured in high-altitude balloons at the same time that VLF emissions were detected on the ground. During a long period of enhanced activity a one-to-one correlation was found between short bursts (approximately $\frac{1}{2}$ s in length) of X rays and bursts of VLF emissions. The excess X ray count rate distribution was consistent with an exponential primary electron energy spectrum of the form

$$J(>E) \simeq 10^6 e^{-E/E_0} \text{ cm}^{-2} \text{ s}^{-1} \quad (1)$$

where $E_0 = 45$ keV.

Rosenberg et al. [1971] concluded that the flux of (1) represented a backscattered flux from the northern hemisphere. If a typical backscatter ratio of about 1 : 10 was used, the precipitated flux in the northern hemisphere would have been of the

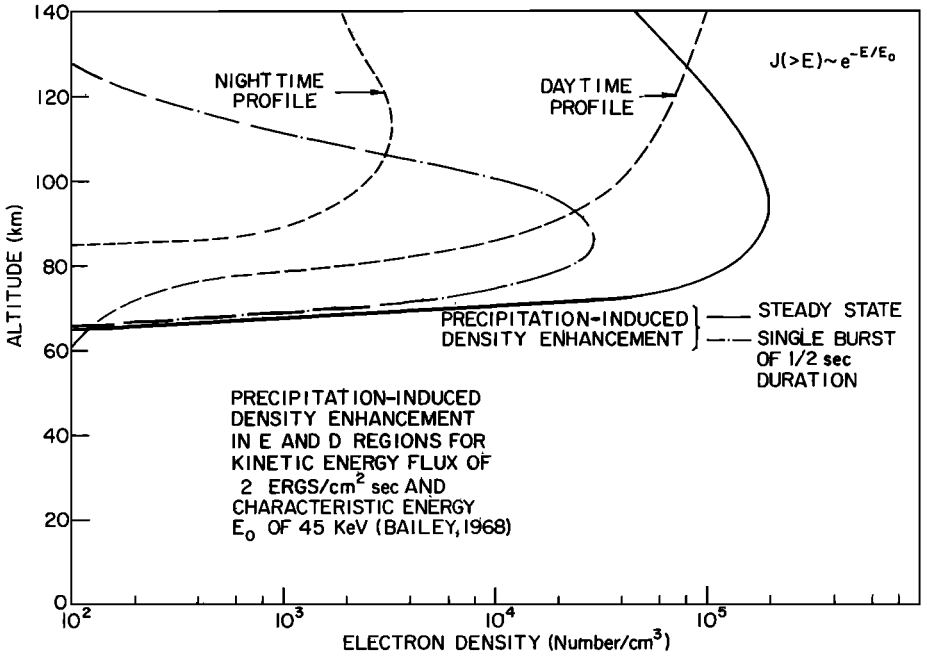

Fig. 4. Precipitation-induced ionization density enhancements.

order of

$$J(>E) \simeq 10^7 e^{-E/E_0}\ \text{cm}^{-2}\ \text{s}^{-1} \tag{2}$$

resulting in an energy deposition rate of approximately 2 erg/cm² s, approaching that of a moderate aurora.

Recent experience has shown that Siple transmitter pulses can readily trigger emissions similar in strength and frequency content to those reported by *Rosenberg et al.* [1971]. Although emission stimulation does not necessarily imply significant precipitation, it is perhaps not unreasonable to suppose that the flux given in either (1) or (2) may resemble that which can be produced by a VLF ground transmitter. For the sake of argument we will assume that this is the case. Since we cannot substantiate this assumption, our aim will not be to show that ULF waves can be generated by a VLF ground transmitter but rather to assess the feasibility of the idea.

Density and Conductivity Enhancements

The ionospheric density enhancement produced by the flux in (2) can be estimated by using some results from a paper by *Bailey* [1968] in which he plots the ion pair production rate as a function of altitude for precipitation fluxes with an exponential form similar to (2). This precipitation-induced density enhancement is shown in Figure 4 both for the case of a single ½-s long burst of particles and also for the steady state case in which it is assumed that the flux of (2) is continuous in time.

From the figure it is clear that a single ½-s burst of precipitated particles will produce a significant perturbation in the normal nighttime ionospheric electron density over the altitude range 60–110 km. In the daytime the significant range of perturbation is approximately 60–100 km.

The density enhancement associated with the precipitation burst results in an enhancement of conductivity, which is shown as a function of altitude in Figure 5 for both the Hall (σ_2) and Pedersen (σ_1) conductivities. The enhancements were calculated by using the ionospheric parameters given by *Hanson* [1961] for average nighttime conditions. Enhancements for average daytime conditions are similar. The height-integrated conductivity enhancements for the Pedersen and Hall conductivities have the values

$$\Delta\Sigma_1 = \int \Delta\sigma_1\, dh \simeq 0.3\ \text{mho}$$
$$\Delta\Sigma_2 = \int \Delta\sigma_2\, dh = 1.5\ \text{mhos} \tag{3}$$

The conductivity enhancement calculated above will persist in the perturbation region until recombination and attachment effects significantly reduce the density enhancement toward the ambient levels. We assume that these effects are governed by the well-known relation

$$dN/dt = q - \Psi N^2 \tag{4}$$

where N is the electron density, q is the volume rate of production of electron-ion pairs, and Ψ is the effective loss coefficient for electrons. For simplicity we assume that Ψ is independent of N and q and has the constant value $\Psi = 6 \times 10^{-7}$ cm³/s. This value for Ψ appears to be reasonable for the 70- to 110-km altitude range in the ionosphere [*Bailey*, 1968; *Watt et al.*, 1974; *Swider and Dean*, 1975].

It is of interest to determine the time behavior of N and subsequently of $\Delta\sigma_{1,2}$ by using (4) for the case in which the VLF transmitter injects a series of identical pulses with period

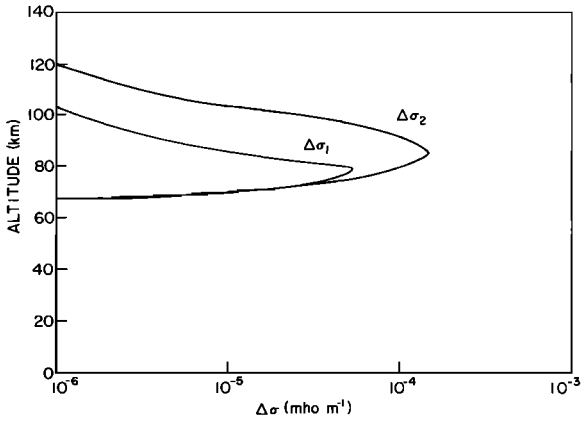

Fig. 5. Conductivity enhancement associated with a ½-s precipitation burst.

T into the magnetosphere. We assume that each induced burst of precipitated particles is impulsive in nature, that each burst conforms to (2), and that each burst enters the same volume of the ionosphere and produces identical enhancements (as is shown in Figure 5). Given this assumption, it is found for large t that the total conductivity enhancement $\Delta\sigma^T$ has both a steady ($\Delta\sigma_{1,2}^s$) and a fluctuating ($\Delta\sigma_{1,2}^f$) component:

$$\Delta\sigma_{1,2}^T(h, t) \simeq \Delta\sigma_{1,2}^s(h) + \Delta\sigma_{1,2}^f(h, t) \tag{5}$$

where h is altitude and where

$$\Delta\sigma_{1,2}^s(h) \simeq \Delta\sigma_{1,2}(h)[\tfrac{1}{2} T\Psi N_0(h)]^{-1/2}$$
$$\Delta\sigma_{1,2}^f(h, t) \simeq \Delta\sigma_{1,2}(h)[\tfrac{1}{2} + m - (t/T)] \tag{6}$$
$$(m+1) \geq t/T \geq m \qquad m = 0, 1, 2, 3, \cdots$$

The quantities $\Delta\sigma_{1,2}(h)$ in (6) are the enhanced Pedersen and Hall conductivities as shown in Figure 5. The quantity $N_0(h)$ is the single-burst electron density enhancement as shown in Figure 4. Equations (6) are valid only at altitudes for which $N_0(h)$ is much larger than the ambient ionization levels. From Figure 4 it can be seen that this limits the region of validity to altitudes below about 100 km. For altitudes between 80 and 100 km, $N_0(h) \sim 3 \times 10^4$ cm⁻³ and $\Delta\sigma_{1,2}^s(h) \simeq 10\Delta\sigma_{1,2}(h)$ for $T = 1$ s. Over this altitude range the length of time t_w necessary to reach the state described by (5) and (6) has the value $t_w \sim [(1/2T)\Psi N_0(h)]^{-1/2} \sim 10$ s.

The horizontal area over which these conductivity enhancements can be produced may be large. For instance, results from the first year of VLF transmissions from Siple Station indicate that the transmitter can illuminate those magnetic field lines whose end points are within 500 km of the transmitter location. If precipitation can be induced on the majority of these field lines, the scale of the region of enhancement may be as large as 1000 km.

Ambient Electric Field

The ambient ionospheric electric field $\mathbf{E}_0$ is one of the most important quantities of our model. This field provides the basic driving force for current flow through the perturbation region and along $\mathbf{B}_0$. Experimentally, the magnitude of $\mathbf{E}_0$ has been found to vary with latitude, time of day, and degree of magnetic disturbance. Within the plasmasphere at mid-latitudes, values of the east-west component of E_0 inferred from whistler measurements (mapped from the equatorial plane) range from 0.5 mV/m during periods of prolonged quiet up to

20 mV/m in the dusk sector during substorm activity [*Carpenter*, 1970]. Slightly inside the plasmapause, combined whistler and balloon measurements [*Mozer et al.*, 1974] have indicated values of E_0 in the range 1–10 mV/m during a period of quieting following a day of moderate disturbance. At higher latitudes, barium cloud releases [*Föppl et al.*, 1968; *Wescott et al.*, 1969], incoherent scatter experiments [*Banks et al.*, 1974; *Carpenter and Kirchoff*, 1975], and satellite dc electric field measurements [*Cauffman and Gurnett*, 1971] commonly give values of E_0 ranging from 2 to 100 mV/m, the higher values being associated with substorm activity. For the purpose of the present discussion we assume that the induced particle precipitation takes place somewhat outside the plasmapause and during a quieting period following a magnetic storm when $E_0 \sim 10$ mV/m.

RESULTS

Given the model discussed above and in Appendix A, we wish to estimate the magnetic field fluctuations that might be measured by a ground observer during an induced particle precipitation experiment. We assume that the VLF transmitter has been in operation for a period of minutes and has been periodically inducing the precipitation of energetic electrons during this time. The enhanced conductivity in the perturbation region has reached the asymptotic value given by (5) and (6). The dc component of the conductivity $\Delta\sigma_{1,2}^s$ will give rise at the ground to a dc perturbation in $\mathbf{B}$, $\Delta\mathbf{B}^s$. Given that the horizontal scale of the perturbed region is 200 km or larger and that the ground observer is beneath this region, the magnitude of $\Delta\mathbf{B}^s$ will have the value $|\Delta\mathbf{B}^s| \simeq \mu_0 \Delta J^s$, where ΔJ^s is given in (B5) of Appendix B. Parameters for the model calculations are listed in the tabulation below.

Parameter	Value
ψ	6×10^{-7} cm^{-3} s^{-1}
Σ_1^a	0.05 mho
Σ_1^s	3 mhos
Σ_1^f	0.3 mho
Σ_1^c	6 mhos
$\|\mathbf{E}_0\|$	10^{-2} V/m
Σ_2^a	0.25 mho
Σ_2^s	15 mhos
Σ_2^f	1.5 mhos
Σ_2^c	9 mhos

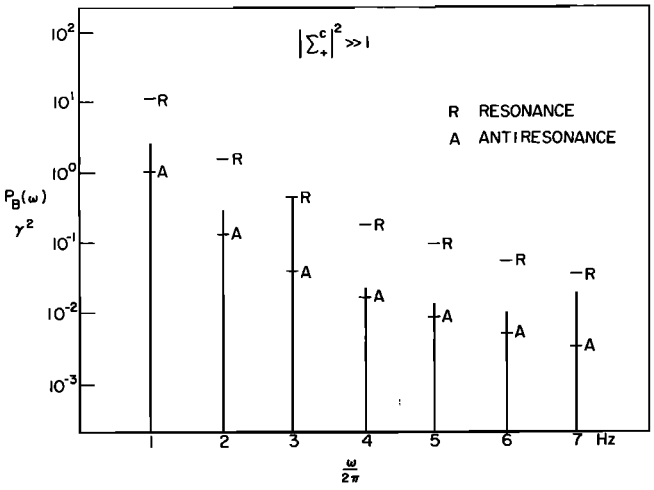

Fig. 6. Power $P_B(\omega)$ of stimulated ULF waves for the case of moderate current flow from the conjugate ionosphere. Units of $P_B(\omega)$ are in terms of 10^{-10} G^2, i.e., γ^2. The transmitter pulse repetition period is 1 s.

Using the parameters listed above (daytime conditions in conjugate ionosphere, nighttime in perturbed ionosphere) we find

$$|\Delta B^s| \simeq 100\ \gamma \tag{7}$$

A perturbation of this magnitude would be readily detectable by magnetometers commonly used at the present time which have sensitivities of approximately $10^{-3}\ \gamma$.

The power distribution in the ac perturbation (i.e., the ULF wave field) that would be observed on the ground under the perturbed region is given by (A13). This equation represents an infinite series made up of power coefficients for each wave component of frequency m/T, where m is a positive integer.

Using the parameters in the tabulation above we have plotted in Figure 6 the power distribution $P_B(\omega)$ in the ac component of $\Delta\mathbf{B}$ (i.e., $\Delta\mathbf{B}^f$) for the case in which $T = 1$ s. The units of $P_B(\omega)$ are γ^2 ($\gamma = 10^{-5}$ G). The solid bars in Figure 6 represent the power in $\Delta\mathbf{B}^f$ at the integer frequencies 1–7 Hz. There is no power at intermediate frequencies, since the system is assumed to be periodic with period T. Like most transmission lines the ULF transmission line discussed here has both a resonance and an antiresonance condition for which the wave amplitude at the input point reaches a maximum (resonance) or a minimum (antiresonance). In general, each harmonic component of frequency m/T will have its own unique resonant/antiresonant condition which, given the parameters of the tabulation above, depends only upon the wave frequency, the length of the transmission line, and the plasma parameters (gyro and plasma frequencies) along the line. Since the latter two quantities are known only roughly, in an actual experimental situation the amplitudes of the bulk of the harmonic waves would probably be neither at their maximum nor their minimum value but somewhere in between. To reflect this uncertainty, we have indicated in Figure 6 the resonance (R) and antiresonance (A) power values for each harmonic wave. In addition, the solid bars represent the power in the harmonic components for the special case in which the third harmonic is at its resonance value. This special case illustrates a distribution that could conceivably arise in an experimental situation [e.g., *Willis and Davis*, 1976]. Note that the amplitude of the fundamental and the first two harmonics is approximately 1 γ, a readily measurable value. Also note that the antiresonance curve, which gives the minimum value for each component, gives an amplitude greater than 30 mγ even for the seventh harmonic at 7 Hz.

The ULF wave amplitudes given in Figure 6 were calculated by assuming daytime conditions in the conjugate ionosphere. This gives a reasonable current flow between hemispheres in the steady state condition. A counter assumption might be that very little current flows between hemispheres. This situation might occur if the conjugate ionosphere is in a nighttime condition of low conductivity or if anomalous resistivity [*Kindel and Kennel*, 1971] or a plasma double layer [*Block*, 1972] has prevented significant current flow from building up. This low current flow condition is explored in Figure 7, where we have plotted the power of the ULF waves for the case $\Sigma_\pm^c \simeq 0$. All other parameters are as they are in the tabulation above, and $T = 1$ s. The curves in Figure 7 are similar to those of Figure 6. Once again the solid bars represent the special case in which the third harmonic is at its resonance value. We note that the power in the waves is about 2 orders of magnitude lower than that shown in Figure 6. However, even at its antiresonance point the amplitude of the fundamental is greater than 30 mγ.

Both Figures 6 and 7 were plotted for the case $T = 1$ s. A

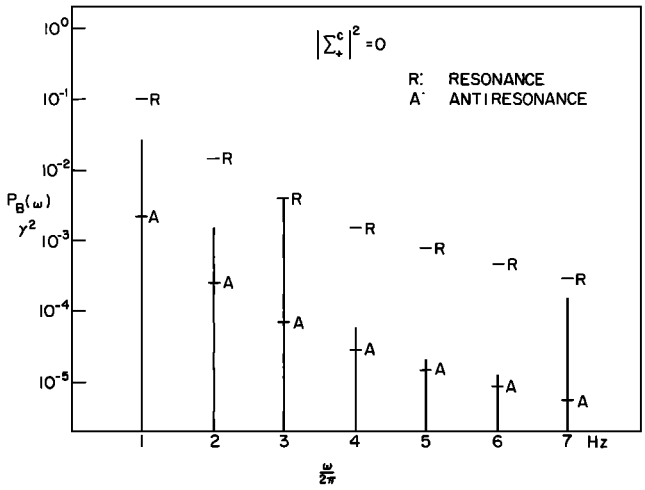

Fig. 7. Power $P_B(\omega)$ of stimulated ULF waves for the case of zero current flow from the conjugate ionosphere. The transmitter pulse repetition period is 1 s.

question of interest concerns the variation of ULF wave power as a function of the pulse period T. This relationship is illustrated in Figure 8, where the power of the ULF component at the fundamental frequency ($1/T$) is plotted versus T. In this plot the parameters of the tabulation apply with the exception of Σ^c, as is noted in the figure. It can be seen that the power in the fundamental wave is a slowly increasing function of T for $T \geq 5$ and a rapidly decreasing function for $T \leq \frac{1}{2}$. Despite the fact that the power in the fundamental increases with T, the power at any fixed frequency generally decreases rapidly with T. As an example of this feature, the envelope of the power in the component at 1 Hz is shown in the figure. It can be seen that the power at 1 Hz is down by 30 dB for $T = 10$ s, in comparison to what it is at $T = 1$ s. It can also be seen that the power in the low current flow case, i.e., $\Sigma_\pm^c \simeq 0$, is always substantially lower than in the high current flow case $|\Sigma_\pm^c| \gg 1$ (actual value used for $\Sigma_\pm^c$ is given in the tabulation).

As a final example of the predictions of our model we present in Figure 9 a plot of the power of the ULF component at the fundamental frequency of 1 Hz versus the magnitude of the periodic precipitated flux. In this figure we hold the spectral form of the flux constant in keeping with (1) and (2) but vary the magnitude of the total flux J_0. It can be seen that the ULF power is a slowly increasing function of J_0 for $J_0 > 10^6$ but a rapidly decreasing function for $J_0 < 10^6$. This is true for both the high and low current flow cases. It is of interest to note that the power is approximately the same for both the high and low current flow cases for $J_0 \leq 10^5$. This situation results from the fact that at these low flux levels the enhancement in conductivity in the perturbation region is small and the maximum current that can be drawn from the conjugate ionosphere is also small, albeit greater than zero. We note that even at low flux levels, $J_0 \sim 10^5$ and the ULF amplitude at the 1-Hz fundamental is 10 mγ, a readily measurable value.

Discussion

Given that the VLF transmitter-induced precipitation flux resembles (1) or (2), our model predicts ULF wave amplitudes in the range of 10–10^3 mγ at the low-altitude boundary of the perturbed region. If the horizontal scale of the perturbed region is 200 km or more, these amplitudes would also prevail on the ground under the perturbation region. Since ULF wave amplitudes of 10–10^3 mγ are readily measurable, it appears feasible that a ground-based VLF transmitter can stimulate ULF waves through the mechanism of controlled energetic particle precipitation. Furthermore, it would appear that a test of our model could be made straightforwardly by using a facility such as Siple Station, where a high-power VLF transmitter is available and where ULF wave measurements are routinely recorded. In fact, data to test the present theory have been and are presently being acquired both at Siple Station and at its conjugate, Roberval, Quebec. The results of the early experiments have been outlined in a recent paper [*Fraser-Smith and Cole*, 1975] which reports that during a week in September of 1973, when the Siple VLF transmitter program was designed to stimulate ULF waves, it was found that all ULF Pc 1 pulsations that occurred during the experiment started during intervals of transmitter operation. Furthermore, the average rate of occurrence of the ULF activity was about twice the rate observed on days with no transmissions.

Fraser-Smith and Cole also found that the frequency structure, duration, and other characteristics of the Pc 1 events appeared to be independent of the VLF transmissions, and, in particular, the average frequencies of the Pc 1 events bore no apparent relation to the pulse repetition frequency of the VLF waves. On this basis they concluded that their data did not support either an early version of the present theory [*Bell*, 1972] or an alternative theory involving parametric interaction between whistler mode waves [*Harker et al.*, 1974].

A similar experiment involving the U.S. Navy VLF transmitter at Cutler, Maine (NAA), has produced interesting but somewhat different results. *Willis and Davis* [1976] have reported the results of a month-long experiment during which NAA was square wave modulated at frequencies of 0.2, 1, and 5 Hz ($T = 5$, 1, 0.2 s), and a network of sensitive magnetometers was employed as ULF detectors. According to the authors, under favorable magnetospheric conditions, otherwise natural-appearing ULF waves (micropulsations) may be induced or enhanced at a harmonic of the transmitter modulation frequency.

Other similar experiments have also been reported recently [*Koons et al.*, 1974; *Reasoner*, 1974]. From the experimental data it seems reasonably clear that waves from VLF transmitters, under favorable circumstances, can stimulate ULF waves. The theory outlined in the present paper provides a direct method of producing ULF waves at a frequency equal to the transmitter pulse repetition rate and harmonics thereof. The possibility for resonance excitation of any of the harmonic

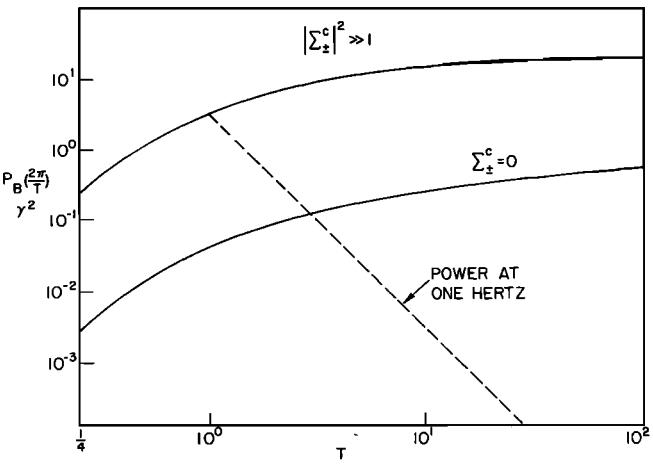

Fig. 8. ULF wave power $P_B(\omega)$, at the fundamental frequency $\omega = 2\pi/T$, plotted as a function of pulse-repetition period T.

modes on the VLF transmission line means that the dominant mode is not necessarily at the fundamental but can be at a higher harmonic. This feature is in agreement with the observations of *Willis and Davis* [1976]. However, the purpose of the present paper is not to show that our particle precipitation mechanism has been responsible for producing ULF waves but rather to assess the feasibility of the idea. It is our opinion that the idea is feasible. Whether the mechanism is presently producing ULF waves is uncertain.

In principle, our mechanism can produce much larger Pc 1 ULF wave amplitudes than have been predicted for other generation schemes. For instance, the radio wave heating technique outlined by *Willis and Davis* [1973] is estimated to produce a maximum ULF wave field of about 5–15 mγ at ground level. The *Harker et al.* [1974] parametric amplification technique is estimated to produce a 2- to 5-mγ field. Finally, the direct radiation techniques which involve huge ground-based antennas [*C. Greifinger*, 1972; *Fraser-Smith et al.*, 1972; *Greifinger and Greifinger*, 1974] are estimated to produce wave fields of the order of 10 mγ. Thus if the particle precipitation technique can be successfully applied, it should offer significant advantages to the ULF experimenter.

In the event that the horizontal scale of the precipitation region is significantly less than we have assumed (200 km), the ULF amplitude prevailing at ground level will be reduced. For instance, if the horizontal cross section of the perturbed region is circular with a diameter as small as 40 km, then P_B at ground level will be reduced 30 dB below the values shown in Figures 6–9. For diameters D of 40 km or smaller, $P_B \propto D^4$; and thus in order to produce a measurable signal at the ground the horizontal scale of the perturbed region must be at least 10 km.

Another factor which influences our results is the recombination coefficient. Although for our calculations we have chosen a value $\Psi = 6 \times 10^{-7}$ cm³/s, it is possible in practice that the effective value of Ψ could be much larger than this (although not much smaller). In our model the main effect of Ψ is in determining the steady state values of enhanced conductivity, current flow, and driving electric field in the perturbed region (a secondary effect concerns the damping of one of the normal modes). For large values of Ψ it can be shown that P_B depends upon Ψ mainly through the dependence of P_B on the driving electric field $\mathbf{E}^s$. According to (B4), $\mathbf{E}^s$ increases as Ψ increases, and since $P_B \propto |E^s|^2$, P_B also increases as Ψ increases. For example, if we pick $\Psi = 6 \times 10^{-6}$ cm³/s, a value 10 times that used in our model, we find through (A13) that the new values of P_B for $|\Sigma_\pm^c|^2 \gg 1$ are approximately a factor of 2 larger than those shown in Figures 6, 8, and 9 and for $|\Sigma_\pm^c| \approx 0$, a factor of 10 larger than those shown in Figures 7, 8, and 9.

The increase of P_B with Ψ makes sense physically. Larger Ψ results in smaller $\Delta\sigma^s$, leading to a reduction in the polarization field and an increase in the total driving field in the perturbation region, leading to increased current flow and higher wave amplitudes.

As was mentioned above, in order to maximize the ULF wave amplitude produced by the particle precipitation it is necessary to draw a moderate current along the earth's magnetic field lines from the conjugate region. If this current is not available, the ULF wave amplitudes, although apparently still easily measurable, are reduced by approximately an order of magnitude. This behavior is illustrated in Figures 6 and 7. At least two factors can serve to limit the parallel current flow along the magnetic field lines linking the perturbed and conjugate regions. One of these is the presence of a region of anomalous resistivity [*Swift*, 1965; *Kindel and Kennel*, 1971], and the other is the presence of a double layer [*Carlqvist and Boström*, 1970; *Block*, 1972; *Carlqvist*, 1972; *Boström*, 1974]. In theory, either of these factors can conceivably limit parallel current flows to maximum values of 10^{-5}–10^{-6} A/m², and these theoretical results compare well with experimental measurements of Birkeland currents at auroral latitudes which tend to show maximum current densities of a few times 10^{-5} A/m² [*Anderson and Vondrak*, 1975].

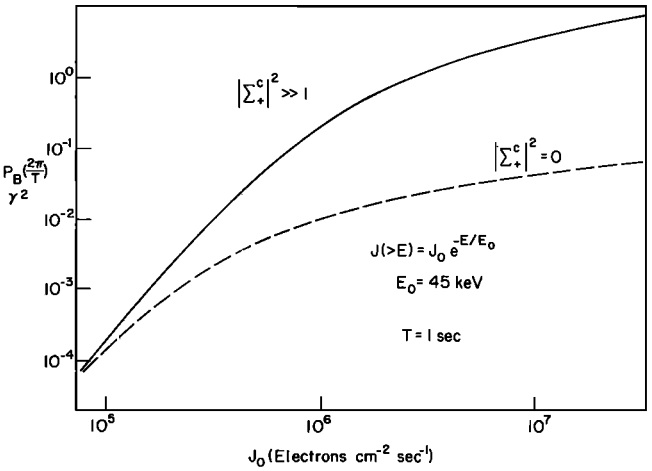

Fig 9. ULF wave power $P_B(\omega)$, at 1 Hz, plotted as a function of the magnitude of the periodic precipitated flux J_0. The pulse-repetition rate is 1 s.

In view of this apparent limitation on parallel current flow in the auroral region it is of interest to estimate the steady state current density required in our model to produce the maximum ULF wave amplitude. From the steady state relation (8) and the tabulation of parameters used we find that in the perturbed region the total field-aligned current per unit of horizontal distance perpendicular to the flow is approximately 7×10^{-2} A/m. Taking account of the finite conductivity of the ionosphere, the radiation pattern of the ground transmitter, the distributed nature of the VLF wave fronts in the magnetosphere, and the effects of convective drifts, we estimate that there must be a transition region of the order of 10 km or more surrounding the perturbation region in which the ionization gradually builds up from the ambient levels to the levels prevailing inside the perturbation region. The bulk of the field-aligned current will flow in this transition region, and the mean current density there would be roughly 10^{-5} A/m², somewhat below the typical maximum values measured in the auroral regions. Thus in practice the phenomena of anomalous resistivity and double layers may not have an important effect upon the ULF wave generation mechanism proposed here.

Another factor which may affect the magnitude of the stimulated ULF waves is the presence of finite perpendicular conductivity in the magnetosphere due to the energetic particle population. One effect of this finite perpendicular conductivity is to reduce any polarization field that exists across the transmission line boundaries, the effective driving electric field in the perturbation region thus being increased and the amplitude of the stimulated ULF waves thereby being increased.

A second and perhaps more important effect of the energetic particle population is to amplify the transmission line waves. The amplification of Pc 1 ULF waves in the magnetosphere is thought to proceed via a cyclotron interaction with energetic

protons [*Jacobs*, 1970]. Amplifications of 20 dB have been estimated for this interaction, and if those estimates are correct, the final amplitudes of the transmission line waves could conceivably be quite different from those shown in Figures 6 and 7. In particular, the dominant mode would perhaps be more a function of the amplification mechanism than of the transmission line resonance conditions.

Although our discussion has been devoted primarily to effects that can be produced by VLF ground-based transmitters, it should be noted here that our model can apply equally well to the case of a satellite-based VLF transmitter. In fact, as is indicated in Figure 1, a satellite-based transmitter can operate close to the emission generation region near the equatorial plane and even at low power outputs can conceivably create a much larger flux of precipitated particles than a more powerful and distant ground-based transmitter.

At low altitudes a satellite-based VLF transmitter should still enjoy significant advantages over ground-based transmitters in experiments to precipitate energetic particles. For example, a good portion of the radiation from a ground transmitter is lost in the earth-ionosphere wave guide and does not enter the magnetosphere. Thus the satellite transmitter would make more efficient use of the available power. Furthermore, the satellite transmitter can stimulate a much wider range of wave normal angles in the magnetosphere than can a ground-based transmitter. This capability significantly expands the options available for maximizing the precipitated flux.

It is our expectation that ongoing ground-based VLF wave injection experiments at Siple and elsewhere will serve to establish the practicality of ideas such as those outlined here. This in turn will lead to improved second-generation experiments which can be carried out both from the ground and from space stations such as the Atmospheric, Magnetospheric, and Plasmas in Space (AMPS) Laboratory. Hopefully, in this process the goals discussed in the introduction will be achieved.

APPENDIX A

Transmission line equations. Figure 3 shows a two-dimensional schematic representation of our proposed ULF transmission line. This line possesses distributed inductance L and capacitance c which vary with position along the earth's magnetic field lines. The equations which describe the propagation of waves along the transmission line (i.e., through the ionosphere and magnetosphere) are the following:

$$\nabla \times \mathbf{E} = -\partial \mathbf{B}/\partial t \tag{A1}$$

$$\nabla \times \mathbf{B} = c^{-2}\partial \mathbf{E}/\partial t + \mu_0 \mathbf{j} \tag{A2}$$

$$\mathbf{j} = N_e(\mathbf{v}_i - \mathbf{v}_e) \tag{A3}$$

$$d\mathbf{V}_{i,e}/dt = \eta_{i,e}[\mathbf{E} + \mathbf{V}_{i,e} \times \mathbf{B}_0] - \nu_{i,e}\mathbf{V}_{i,e} \tag{A4}$$

where the first two equations are Maxwell's, the third defines the current density for a two-component plasma consisting of an equal number N of electrons e and ions i, and the last is the linearized transport relation for the charge carriers (assumed to be of zero temperature). The quantities $\mathbf{V}_{i,e}$, $\eta_{i,e}$, and $\nu_{i,e}$ are the velocity vectors, the charge-to-mass ratios, and the effective collision frequencies of the ions and electrons, respectively. The quantity $\mathbf{B}_0$ is the earth's magnetic field. In general, the conductivity along $\mathbf{B}_0$ is always very large in comparison to the conductivity perpendicular to $\mathbf{B}_0$. For simplicity we assume that the parallel conductivity is infinite and that $\mathbf{E} \cdot \mathbf{B}_0 = 0$. Thus equations (A1)–(A4) will apply only to the transverse component of E, i.e., $\mathbf{E}_\perp$.

Perturbation region. The perturbation region lies in an altitude range of the ionosphere where, for ULF, collisional effects dominate wave effects, i.e., $\nu_{i,e} \gg \omega$. In this case the term $dV_{i,e}/dt$ can be neglected in (A4). In the steady state regime both a steady and fluctuating component of current will be drawn along $\mathbf{B}_0$, and E and B on the transmission line will also possess both a steady and fluctuating component. In the case of E the steady component arises because of polarization charges along the boundaries of the transmission line, and the polarization field due to these charges acts to reduce the total electric field in the perturbation region. The steady components of the fields are related through the expression

$$\nabla \times \mathbf{B}_s = \mu_0 \hat{\sigma}_s \cdot \mathbf{E}_s$$

To simplify the equations for the fluctuating components of the ULF fields, we assume that $\mathbf{B}_0$ is vertical in the perturbation region and that the horizontal components of the ULF fields in the perturbation region can adjust instantaneously at any given altitude to changes in current flow that may occur because of particle precipitation effects. This amounts to a quasi-static condition on $\mathbf{E}_f$ in the horizontal plane, i.e., $\nabla_\perp \times \mathbf{E}_f = 0$, or

$$E_{fx}/\partial y = E_{fy}/\partial x \tag{A5}$$

By combining (A1)–(A5) a wave equation can be written for $\mathbf{E}_f$ in terms of the two normal modes $E_\pm = (E_{fx} \pm iE_{fy})$

$$\left[\frac{\partial^2}{\partial z^2} - c^{-2}\frac{\partial^2}{\partial t^2} - \mu_0\sigma_\pm \frac{\partial}{\partial t} - \mu_0 \frac{\partial \sigma_\pm}{\partial t}\right] E_\pm = \mu_0 \frac{\partial}{\partial t}(\sigma_\pm^{\,f} E_\pm^{\,s}) \tag{A6}$$

where z is along the vertical, $\sigma_\pm = \sigma_\pm^{\,s} + \sigma_\pm^{\,f}$, $\sigma_\pm^{\,s} = \sigma_1^{\,s} \pm i\sigma_2^{\,s}$, $\sigma_\pm^{\,f} = \sigma_1^{\,f} \pm i\sigma_2^{\,f}$, $E_\pm^{\,s} = E_x^{\,s} \pm iE_y^{\,s}$, and the steady s and fluctuating f components of the Pedersen and Hall conductivities, σ_1 and σ_2, can be found from (6). Equation (A6) describes the excitation and propagation of transmission line waves through the perturbation region. In general, it is difficult to solve because of the temporal and spatial variation of $\sigma_\pm$. To simplify the calculations, we make a slab approximation of the enhanced conductivity profile in the perturbed region (Figure 5) and assume that the enhanced conductivities are constant throughout a height range of ± 10 km about their maxima and zero elsewhere. In this approximation we have from (3)

$$\begin{aligned} \Delta\sigma_1(h) &\simeq 1.5 \times 10^{-5} \text{ mho/m} \\ \Delta\sigma_2(h) &\simeq 7.5 \times 10^{-5} \text{ mho/m} \end{aligned} \tag{A7}$$

In addition, we approximate the quantity $\sigma_\pm$ by its steady state value of $\sigma_\pm^{\,s}$. This approximation is reasonable if $|\sigma_\pm^{\,s}| \gg |\Delta\sigma_\pm^{\,f}|$, an inequality which holds for the parameters of our model. Furthermore, we neglect all ionospheric drift effects. With these approximations, (A6) can be solved for $E_\pm$ through the use of elementary methods.

Magnetosphere. In the magnetospheric portion of the ULF transmission line it is generally true that collisional effects are unimportant and that source currents, such as those on the right-hand side of (A6), are absent. If it is also the case that curvature of the earth's magnetic field lines is negligible on the scale of a wavelength, then (A1)–(A4) yield the following equations for ULF transverse electromagnetic (TEM) waves on the transmission line in the limit $\omega \to 0$:

$$\frac{\partial^2 E_\pm}{\partial z^2} - V_A^{-2}\frac{\partial^2 E_\pm}{\partial t^2} = 0$$
$$\left(\frac{\partial}{\partial x} \pm i\frac{\partial}{\partial y}\right)E_\pm = 0 \qquad \text{(A8)}$$

where the second relation is the normal mode analog to Laplace's equation, where (A5) holds; z is the distance measured along $\mathbf{B}_0$; and V_A is the local Alfvén velocity, assumed to depend upon z alone. Since, in general, for wave frequencies in the Pc 1 range the fractional change in V_A in the space of a wavelength is small, a WKB solution to (A8) should suffice to describe the ULF wave structure.

The use of (A8) is predicated upon the assumption that only the transmission line TEM mode is important. If higher-order modes are considered, the equations for oblique propagation must be used with attendant complications [*P. Greifinger*, 1972]. A TEM mode structure appears appropriate at low altitudes. However, at high altitudes the differential phase shift between the normal modes may produce a more complex mode structure.

Conjugate ionosphere. In the conjugate ionosphere, linked by the earth's magnetic field lines to the perturbation region, we assume that (A6) applies with the right-hand side set equal to zero (no sources) and with the conductivity $\sigma_\pm$ set equal to the ambient value $\sigma_\pm{}^c$ appropriate to the local time of interest. The assumption of no sources in the conjugate region cannot strictly be correct, since a fraction ($\sim$10%) of the precipitating electrons in the perturbed region will backscatter and produce periodic enhancements of ionization in the conjugate region as well. However, the strength of the sources in the conjugate region will be comparatively small, and the major effects should be produced in the perturbation region.

In order to find the ULF wave reflection coefficients at the top of the conjugate ionosphere, we must solve (A6). For nighttime conditions, $\sigma_\pm{}^c$ is quite small, the ionosphere is essentially transparent to ULF waves, and a WKB solution of (A6) will suffice. For daytime conditions the strong height variation of $\sigma_\pm{}^c$ generally necessitates a numerical solution of (A6) [*Greifinger and Greifinger*, 1965]. To avoid this complexity, we derive an approximate relation between $E_\pm$ and $B_\pm$ that holds at the top of the conjugate ionosphere and that allows the reflection coefficient to be obtained. Neglecting the small displacement current, we integrate (A2) from the base to the top of the conjugate ionosphere, assuming that $E_\pm$ varies slowly in this region and noting that because of strong daytime absorption, $B_\pm \simeq 0$ at the base. This procedure yields the relation

$$B_\pm \simeq \pm i\mu_0\Sigma_\pm{}^c E_\pm \qquad \text{(A9)}$$

where $\Sigma_\pm{}^c$ is the height-integrated conductivity. Although (A9) is only a rough approximation, use of it avoids the unwarranted complexity of a full wave solution in the conjugate ionosphere.

Boundary conditions. At the interface between line sections j and k the appropriate boundary conditions are

$$E_\pm{}^k = E_\pm{}^j \qquad \text{(A10)}$$

At each base of the transmission line, i.e., immediately below the perturbed and conjugate ionospheres, we assume that the conductivity is infinite and thus

$$E_{\pm|\text{base}} = 0 \qquad \text{(A11)}$$

Condition (A11) is equivalent to the assumption that the earth's surface is a perfect conductor and that the phase shift of ULF waves between the earth and the ionosphere is negligible. This approximation has been used previously by other authors [e.g., *Jacobs and Watanabe*, 1962; *Prince and Bostick*, 1964], and its validity has been studied in some detail [*Greifinger and Greifinger*, 1965; *Field and Greifinger*, 1965].

For daytime conditions in the conjugate ionosphere the Pc 1 ionospheric transmission coefficients are quite small, and thus (A11) is not a significant boundary condition; instead we use (A9). In addition, at the transverse boundaries of the transmission line, i.e., at the location of the field lines which carry the current, we have

$$\mathbf{n}\cdot(\mathbf{E}_e - \mathbf{E}_i) = \rho^f/\epsilon_0$$
$$\mathbf{n}\times(\mathbf{E}_i - \mathbf{E}_e) = 0$$
$$|\mathbf{n}\times(\mathbf{B}_e - \mathbf{B}_i)| = \mu_0 j^f \qquad \text{(A12)}$$
$$\mathbf{n}\cdot(\mathbf{B}_e - \mathbf{B}_i) = 0$$

where $\mathbf{n}$ is a unit normal pointing outward from the surface defined by the field lines connecting the perturbation region, $\mathbf{E}_{i,e}$ and $\mathbf{B}_{i,e}$ are the interior and exterior solutions for the transmission line electric and magnetic fields, respectively, j^f is the fluctuating current along $\mathbf{B}_0$ at the transmission line boundaries, and ρ^f is the fluctuating surface density of charge on the boundaries.

Finally, in the portion of space exterior to the current-carrying field lines we apply the condition $E_\pm \to 0$ as $r \to \infty$, where r is the horizontal distance from the boundaries of the perturbed region.

Field amplitude. Equations (A6)–(A12) form the complete set necessary to find $E_\pm$ along the transmission line and the current flow in the perturbed and conjugate ionosphere. In solving (A6) for the interior of the perturbed region we assume that the linear approximation is valid and that the conductivities $\sigma_\pm$ and $\sigma_\pm{}^f$ are functions of time alone and do not vary with position. When applying (A6) to the exterior of the perturbed region, we assume that ambient conditions apply, with $\sigma_\pm = \sigma_\pm{}^a$ and $\sigma_\pm{}^f = 0$. For simplicity we assume that the perturbed region resembles a cylindrical section of radius R and height l. As is shown in Appendix B, with this geometry, $\mathbf{E}_s$ is constant in the perturbed region. Thus as can be seen from (A6), $E_\pm$ will not be a function of x or y in the interior region. This fact makes the determination of the field structure in the interior region fairly straightforward.

By using a Fourier transform in the time domain the following solution can be obtained for the power in the ULF perturbation field at the base of the perturbed region:

$$P_B = \mu_0{}^2|E_\pm{}^s|^2|k_\pm|^{-2}|\sigma_\pm{}^f|^2$$
$$\cdot\sum_{N=1}^{\infty}(2\pi N)^{-2}[|G_+(2\pi N/T)|^2 + |G_-(2\pi N/T)|^2] \qquad \text{(A13)}$$

where the term of order m in the series represents the power at the angular frequency $\omega = 2\pi m/T$, where the driving electric field $E_\pm{}^s$ is given in (B4) of Appendix B, where

$$k_\pm = \left[i\omega\mu_0\sigma_\pm{}^a - \frac{\omega^2}{c^2}\right]^{1/2}$$

and where

$$G_{\pm}(\omega) = \tanh\left(\frac{lk_{\pm}}{2}\right)\left\{1 + \left[\cosh(lk_{\pm}) + \frac{i\omega}{V_A k_{\pm}}\left(\frac{1 - R_{\pm}}{1 + R_{\pm}}\right)\sinh(lk_{\pm})\right]^{-1}\right\}$$

$$R_{\pm} \equiv \frac{1 - \mu_0 V_A{}^c \Sigma_{\pm}{}^c}{1 + \mu_0 V_A{}^c \Sigma_{\pm}{}^c} e^{-2i\omega g(s)}$$

where $V_A{}^c$ is the Alfvén velocity at the top of the conjugate ionosphere, s is the field line path length between ionospheres, and $g(s) = \int_0^s V_A{}^{-1}\, dz$.

Appendix B

Horizontal electric field distribution in the ionosphere. In order to determine the VLF transmission line current flow in the ionosphere we need first to determine the steady state electric field distribution in the ionosphere. Continuity of current in both the perturbed and conjugate ionospheres requires

$$\nabla \cdot \mathbf{I} \,/\, J_{\parallel} \tag{B1}$$

where $\mathbf{I}$ is the height-integrated horizontal current density and $J_{\parallel}$ is the field-aligned current density flowing into the ionosphere. By definition we also have

$$\mathbf{I} = \hat{\Sigma} \cdot \mathbf{E}_s \tag{B2}$$

where $\hat{\Sigma}$ is the horizontal height-integrated conductivity tensor and $\mathbf{E}_s$ is the steady state ionospheric horizontal electric field. Since $\nabla \times \mathbf{E}_s = 0$, $\mathbf{E}_s$ is derivable from a scalar potential function ϕ. The equation for ϕ is derived by combining (B1) and (B2) to yield

$$\frac{\partial^2 \phi}{\partial x^2} + \frac{\partial^2 \phi}{\partial y^2} = -J_{\parallel}(\Sigma_1)^{-1} \tag{B3}$$

where Σ_1 is the height-integrated Pedersen conductivity.

The boundary conditions to be applied are the following.

1. The component of $\mathbf{E}$ tangent to the boundary (assumed to be sharp) of the perturbation region is continuous.
2. The component of $\mathbf{I}$ normal to the boundary is discontinuous by the factor $J_{\parallel}$.
3. In the perturbed ionosphere, far from the perturbed region, the current flow is steady at the value $\mathbf{J}_a = \hat{\Sigma}^a \cdot \mathbf{E}_a$, where the ambient field $\mathbf{E}_a$ is assumed to be constant over a large region.
4. In the conjugate ionosphere, far from the field lines linking the perturbed region, the current flow is steady at the value $\mathbf{J}_c = \hat{\Sigma}^c \cdot \mathbf{E}_a$.
5. The conductivity along $\mathbf{B}_0$ is infinite.

In effect, the third and fourth conditions constrain the perturbed and conjugate ionospheres to act as constant current sources.

For explicitness we assume that the perturbed region is roughly circular in cross section with a radius R. In this case the solution for ϕ can be readily obtained, and it is found that the field inside the perturbation region is constant and is deviated in direction by an angle $\psi = \tan^{-1}[(\beta - \eta)/(\alpha - \gamma)]$ from the direction of the ambient field $\mathbf{E}_a$.

The amplitude of the field has the value

$$|\mathbf{E}_i| = 2\gamma[(\alpha + \gamma)^2 + (\eta - \beta)^2]^{-1/2}|\mathbf{E}_a| \tag{B4}$$

where $\alpha = \Sigma_1{}^s + \Sigma_1{}^c$, $\beta = \Sigma_2{}^s + \Sigma_2{}^c$, $\gamma = \Sigma_1{}^a + \Sigma_1{}^c$, and $\eta = \Sigma_2{}^a + \Sigma_2{}^c$. The total enhanced current in the perturbation region due to the electric field described by (B3) can be found from the relation $\Delta J^s = |\Sigma^s \cdot \mathbf{E}_i - \Sigma^a \cdot \mathbf{E}_a|$, or

$$\Delta J^s = (\gamma^2 + \eta^2)^{1/2}\left[\frac{(\alpha - \gamma)^2 + (\eta - \beta)^2}{(\alpha + \gamma)^2 + (\eta - \beta)^2}\right]^{1/2}|\mathbf{E}_a| \tag{B5}$$

Acknowledgments. I wish to express my appreciation for the many helpful and stimulating discussions that I held with my colleagues at the Radioscience Laboratory during the course of this research. Special thanks go to J. P. Katsufrakis, without whom the Siple facility would not be a reality. This research was sponsored in part by the National Aeronautics and Space Administration under grant NGL-008 and in part by the Advanced Research Projects Agency of the Department of Defense under contract N00014-75-C-1095.

The Editor thanks J. C. Foster and D. L. Reasoner for their assistance in evaluating this paper.

References

Anderson, H. R., and R. R. Vondrak, Observations of Birkeland currents at auroral latitudes, *Rev. Geophys. Space Phys., 13,* 243, 1975.

Bailey, D. K., Some quantitative aspects of electron precipitation in and near the auroral zone, *Rev. Geophys., 6,* 289, 1968.

Banks, P. M., C. L. Rino, and V. B. Wickwar, Incoherent scatter radar observations of westward electric fields and plasma densities in the auroral ionosphere, 1, *J. Geophys. Res., 79,* 187, 1974.

Bell, T. F., The production of micropulsations using VLF transmitters, paper presented at spring meeting, Union Radio Sci. Int., Washington, D. C., April 13–15, 1972.

Block, L. P., Potential double layers in the ionosphere, *Cosmic Electrodynamics, 3,* 349, 1972.

Boström, R., Ionosphere-magnetosphere coupling, in *Earth's Particles and Fields,* edited by B. M. McCormac, D. Reidel, Dordrecht, Netherlands, 1974.

Campbell, W. H., Geomagnetic pulsations, in *Physics of Geomagnetic Phenomena,* vol. 2, edited by S. Matsushita and W. H. Campbell, Academic, New York, 1967.

Carlqvist, P., On the formation of double layers in plasma, *Cosmic Electrodynamics, 3,* 377, 1972.

Carlqvist, P., and R. Boström, Space charge regions above the aurora, *J. Geophys. Res., 75,* 7140, 1970.

Carpenter, D. L., Whistler evidence of the dynamic behavior of the dusk side bulge in the plasmasphere, *J. Geophys. Res., 75,* 3837, 1970.

Carpenter, L. A., and V. W. J. H. Kirchoff, Comparison of high-latitude and mid-latitude ionospheric electric fields, *J. Geophys. Res., 80,* 1810, 1975.

Cauffman, D. P., and D. A. Gurnett, Double-probe measurements of convection electric fields with the Injun 5 satellite, *J. Geophys. Res., 76,* 6014, 1971.

Field, E. C., and C. Greifinger, Transmission of geomagnetic micropulsations through the ionosphere and lower exosphere, *J. Geophys. Res., 70,* 4885, 1965.

Föppl, H., G. Haerendel, L. Haser, R. Lüst, F. Melzner, B. Meyer, H. Neuss, H. Rabben, E. Rieger, H. Stöcker, and W. Stoffregen, Preliminary results of electric field measurements in the auroral zone, *J. Geophys. Res., 73,* 21, 1968.

Foster, J. C., On experimental observation of whistler triggered electron-cyclotron interactions in the magnetosphere, *Tech. Note BN744,* Univ. of Md., College Park, 1973.

Fraser-Smith, A. C., and D. M. Bubenik, The effect of the conducting earth on the micropulsation-generating capability of a ground-based current loop, *J. Geophys. Res., 79,* 1038, 1974.

Fraser-Smith, A. C., and C. A. Cole, Jr., Initial observations of the artificial stimulation of VLF pulsations by pulsed VLF transmissions, *Geophys. Res. Lett., 2,* 146, 1975.

Fraser-Smith, A. C., K. J. Harker, R. T. Bly, Jr., and D. M. Bubenik, Generation of artificial geomagnetic micropulsations with a large ground-based current loop, *Tech. Rep. SEL-72-023,* Stanford Electron. Lab., Stanford Univ., Stanford, Calif., 1972.

Greifinger, C., Feasibility of ground-based generation of artificial micropulsations, *J. Geophys. Res., 77,* 6761, 1972.

Greifinger, C., and P. Greifinger, Transmission of micropulsations through the lower ionosphere, *J. Geophys. Res., 70,* 2217, 1965.

Greifinger, C., and P. Greifinger, Generation of VLF by a horizontal electric dipole, *Radio Sci., 9,* 533, 1974.

Greifinger, P., Ionospheric propagation of oblique hydromagnetic plane waves at micropulsation frequencies, *J. Geophys. Res., 77,* 2377, 1972.

Hanson, W. B., Structure of the ionosphere, in *Satellite Environment Handbook*, edited by F. S. Johnson, pp. 25–46, Stanford University Press, Palo Alto, Calif., 1961.

Harker, K. J., F. W. Crawford, and A. C. Fraser-Smith, Generation of Alfvén waves in the magnetosphere by parametric interaction between whistlers, *J. Geophys. Res., 79*, 1836, 1974.

Helliwell, R. A., and J. P. Katsufrakis, VLF wave injection into the magnetosphere from Siple Station, Antarctica, *J. Geophys. Res., 79*, 2511, 1974.

Helliwell, R. A., J. P. Katsufrakis, and M. L. Trimpi, Whistler-induced amplitude perturbation in VLF propagation, *J. Geophys. Res., 78*, 4679, 1973.

Jacobs, J. A., *Geomagnetic Pulsations*, Springer, New York, 1970.

Jacobs, J. A., and T. Watanabe, Propagation of hydromagnetic waves in the lower exosphere and the origin of short period geomagnetic micropulsations, *J. Atmos. Terr. Phys., 24*, 413, 1962.

Kindel, J. M., and C. F. Kennel, Top side current instabilities, *J. Geophys. Res., 76*, 3055, 1971.

Koons, H. C., M. H. Dazey, and D. A. McPherson, Micropulsations triggered by VLF wave transmissions into the magnetosphere (abstract), *Eos Trans. AGU, 55*, 400, 1974.

Mozer, F. S., R. Serlin, D. L. Carpenter, and J. Siren, Simultaneous electric field measurements near $L = 4$ from conjugate balloons and whistlers, *J. Geophys. Res., 79*, 3215, 1974.

Prince, C. E., Jr., and F. X. Bostick, Jr., Ionospheric transmission of transversely propagated plane waves at micropulsation frequencies and theoretical power spectrums, *J. Geophys. Res., 69*, 3213, 1964.

Reasoner, D. L., Artificial generation of VLF waves with a TVLF transmitter system (abstract), *Eos Trans. AGU, 55*, 401, 1974.

Rosenberg, T. J., R. A. Helliwell, and J. P. Katsufrakis, Electron precipitation associated with discrete very low frequency emissions, *J. Geophys. Res., 76*, 8445, 1971.

Stiles, G. S., and R. A. Helliwell, Frequency-time behavior of artificially stimulated VLF emissions, *J. Geophys. Res., 80*, 608, 1975.

Swider, W., and W. A. Dean, Effective electron loss coefficient of the disturbed daytime *D* region, *J. Geophys. Res., 80*, 1815, 1975.

Swift, D. W., A mechanism for energizing electrons in the magnetosphere, *J. Geophys. Res., 70*, 3061, 1965.

Watt, T. M., L. L. Newkirk, and E. G. Shelly, Joint radar-satellite determination of the effective recombination coefficient in the auroral *E* region, *J. Geophys. Res., 79*, 4725, 1974.

Wescott, E. M., J. D. Stolarik, and J. P. Heppner, Electric fields in the vicinity of auroral forms from motions of barium vapor releases, *J. Geophys. Res., 74*, 3469, 1969.

Willis, J. W., and J. R. Davis, Radio frequency heating effects on electron density in the lower *E* region, *J. Geophys. Res., 78*, 5710, 1973.

Willis, J. W., and J. R. Davis, VLF stimulation of geomagnetic micropulsations, *J. Geophys. Res., 81*, 1420, 1976.

(Received July 21, 1975;
accepted January 28, 1976.)